Journal of Catalysis 279 (2011) 88–102

Contents lists available at ScienceDirect

Journal of Catalysis

journal homepage: www.elsevier.com/locate/jcat

Lowering the synthesis temperature of Ni_2P/SiO_2 by palladium addition

V. Teixeira da Silva [a,*], L.A. Sousa [a], R.M. Amorim [b,1], L. Andrini [c], S.J.A. Figueroa [d,e], F.G. Requejo [c], Flavio C. Vicentini [f]

[a] NUCAT/PEQ/COPPE/Federal University of Rio de Janeiro, Caixa Postal 68502, CEP 21941-972 Rio de Janeiro, RJ, Brazil
[b] Seção de Química, Instituto Militar de Engenharia, CEP 22290-270 Rio de Janeiro, RJ, Brazil
[c] INIFTA and Dto. de Física, Fac. de Ciencias Exactas, Universidad Nacional de La Plata, CONICET, CP 1900 La Plata, Argentina
[d] CINDECA, Dto. Química, Fac. de Ciencias Exactas, Universidad Nacional de La Plata, CONICET, CICPBA, 47 n°257, CP 1900 La Plata, Argentina
[e] European Synchrotron Radiation Facility (ESRF), BP 220, CEDEX 9, CP 38043 Grenoble, France
[f] Laboratório Nacional de Luz Síncrotron (LNLS), Caixa Postal 6192, 13038-970 Campinas, SP, Brazil

ARTICLE INFO

Article history:
Received 14 November 2010
Revised 7 January 2011
Accepted 8 January 2011
Available online 12 February 2011

Keywords:
Nickel phosphide
Thiophene hydrodesulfurization
X-ray near-edge structure

ABSTRACT

The addition of small amounts of palladium (0.1%, 0.5% and 1.0% w/w) to a $Ni_xP_yO_z/SiO_2$ sample led to a decrease of ~200 K in the synthesis temperature of Ni_2P/SiO_2, allowing synthesis to proceed at 723 K. *In situ* X-ray diffraction (XRD) and X-ray absorption near-edge structure (XANES) experiments demonstrated that the phosphate → phosphide transformation started at approximately 673 K, and the total time to reduce the phosphate phase was decreased by the presence of palladium. Based on the *in situ* P K-edge XANES experiments and CO chemisorption uptakes, it was proposed that, depending on the amount of palladium incorporated, the final catalysts present different degrees of reduction, thereby impacting catalytic activity. An increase in activity was observed for the palladium-containing samples during time on stream, which might be associated with the formation of a phosphosulfide active species. The extent of the phosphosulfide species formation was dependent on the degree of reduction.

1. Introduction

Since the early works of Robinson et al. [1] and Li et al. [2] on Ni_2P and MoP, respectively, transition metal phosphides have attracted attention as catalysts for hydrotreating (HDT) reactions because of their exceptional activities. Of all the phosphides reported thus far in the catalysis literature (*e.g.*, MoP [2–7], WP [6–10], Fe_2P [11], and CoP [11,12]), Ni_2P has been the most studied because it shows the highest activity in hydrodesulfurization (HDS) and hydrodenitrogenation (HDN) reactions, even surpassing the activity of the best commercial catalysts [7].

There are several methods for preparing transition metal phosphides, including solid-state reactions between metals and phosphorous [13], the electrolysis of fused salts [14], the solvothermal method [15], the thermal decomposition of metal–phosphine complexes [16] or of single-source molecular precursors [17] and the temperature-programmed reduction (TPR) of phosphates [7]. Among these, only TPR allows the synthesis of transition metal phosphides in supported form, making it the most commonly employed methodology in catalysis.

However, the major drawback of the TPR method for the synthesis of bulk or supported phosphides is related to high temperatures (generally >973 K) required to reduce the P—O bond [5,7,8,18]. For this reason, the development of new synthetic routes for the production of supported Ni_2P at temperatures <973 K has led to different approaches, such as the modification of the precursor from nickel phosphate to nickel hypophosphite [19], nickel dihydrogenphosphite [20] or nickel thiophosphate [21], as well as the use of PH_3/H_2 gas mixtures [22]. Although these new synthetic routes lower the synthesis temperature of supported Ni_2P from 973 K to as low as 423 K [22], there are some disadvantages to their use. For example, the thermal decomposition of hypophosphites in an argon atmosphere proposed by Guan et al. [19] allows the synthesis of both bulk and supported Ni_2P at temperatures of approximately 523 K, but NaCl and HCl are formed as side products. These compounds raise the issue of materials corrosion and the necessity of thoroughly washing the catalyst. Furthermore, the method does not allow the *in situ* synthesis of Ni_2P, and consequently, the catalyst must be synthesized in an autoclave reactor, subjected to a passivation step to allow its manipulation in the atmosphere, loaded in another reactor and suffer reactivation at 773 K under a flow of H_2 prior to use.

Cecilia et al. [20] proposed the use of nickel dihydrogenphosphite supported on MCM-41 instead of nickel phosphate, as a viable alternative to lower the synthesis temperature of Ni_2P. In this method, $Ni(HPO_3H)_2$ was prepared by making a solution with stoichiometric amounts of nickel hydroxide and phosphorous acid. The solution can be either slowly dried to form the precursor of the

* Corresponding author.
E-mail address: victor.teixeira@nucat.coppe.ufrj.br (V.T. da Silva).
[1] Present address: INPI, CEP 20081-240 Rio de Janeiro, RJ, Brazil.

0021-9517
doi:10.1016/j.jcat.2011.01.010

bulk Ni_2P or used to impregnate a silicious support, such as silica, MCM-41 or SBA-15. Using very particular heating rate (β), final temperature, and space velocity conditions, the authors were able to synthesize Ni_2P at 648 K. However, the major disadvantage of this method was related to the low P-to-Ni atomic ratio of 2 because if temperatures lower or higher than 648 K are used in the synthesis (or even during the reaction), then undesired catalytically inactive phases such as Ni_5P_4 and $Ni(PO_3)_2$ are formed.

The largest reduction in synthesis temperature of supported Ni_2P was achieved by Yang and Prins [22], who used a 10% PH_3/H_2 gas mixture and temperatures of approximately 423 K to phosphide Ni/SiO_2 or Ni/Al_2O_3 that were previously reduced at 773 K with pure hydrogen. As a consequence of the low temperatures used to synthesize the Ni_2P phase, the particle size achieved after the reduction step in pure hydrogen was retained, thus allowing the preparation of highly dispersed metal phosphide particles. In addition, as is well documented in the literature, it is difficult to prepare transition metal phosphides supported on alumina by the phosphate method because phosphate ions tend to react with the support, forming an undesired $AlPO_4$ phase that alters the acid–base properties and impacts metal dispersion. However, this negative consequence can be avoided by using the method presented by Yang and Prins [22]. Nevertheless, due to security reasons, the use of phosphine on either laboratory or industrial scales is problematic, making this method difficult to implement.

Despite all efforts that have been made in the last decade, there is not yet a practical way to synthesize supported transition metal phosphides using mild conditions.

Another point that it is not very clear in the phosphide literature concerns the nature of the phosphate phase. In fact, due to its amorphicity, the nature of the nickel phosphate precursor has been a matter of debate, as has its solid-state transformation to phosphide (*i.e.*, phosphate → phosphide). The reason for the apparent contradictory results can be explained by taking into account whether different researchers used diverse P/Ni ratios to synthesize the phosphate precursor and whether this phosphate underwent a calcination step after its synthesis.

Using a P/Ni of 0.5, Stinner et al. [18] concluded that after synthesis, the compound was composed of a mixture of different phosphate species, including $Ni_3(PO_4)_2$ and $NiNH_4PO_4{\cdot}H_2O$, that would afford a mixture of NiO and nickel phosphates of different composition after calcination in air. From ^{31}P NMR data, the authors identified several phosphorous species, such as $H_nPO_4^{1(3-n)-1}$, $P_2O_7^{4-}$, and $(PO_3^-)_n$, and proposed that the transformation of either bulk or supported-on-silica nickel phosphate to nickel phosphide would proceed through the formation of several intermediates (*e.g.*, Ni_3P, $Ni_{12}P_5$, and Ni_5P_2). Moreover, Wang et al. [11] reached similar conclusions to those of Stinner et al. [18] concerning the nature of the phosphate phases and the solid-state transformation from nickel phosphate to nickel phosphide. However, there is now a consensus in the literature that if a surplus of phosphate is not added during the preparation, then after the reduction step, there is no formation of pure Ni_2P but rather formation of a mixture of $Ni_2P + Ni_{12}P_5$ because part of the phosphorous is lost as PH_3.

Wang et al. [11] studied the synthesis of Ni_2P/SiO_2 and concluded that the support did not influence the nickel phosphide phase formation if an excess of phosphorous was used in the phosphate preparation. This conclusion was not shared by Rodriguez et al. [23], who identified NiO and $Ni_{12}P_5$ formation during temperature-programmed synthesis of Ni_2P/SiO_2 using time-resolved XRD, but they did not use an excess of phosphorous. These authors studied the synthesis of unsupported Ni_2P by time-resolved XRD using uncalcined nickel phosphate as a starting material; the authors identified ammonium nickel phosphate, $NiNH_4PO_4{\cdot}H_2O$, by XRD. According to the authors, the transformation of phosphate → phosphide under a flow of 5% H_2/He gas mixture occurred in three steps: (1) from room temperature to 473 K, the diffraction pattern of the nickel ammonium phosphate was retained; (2) from 573 to 673 K, there was an amorphization of the $NiNH_4PO_4{\cdot}H_2O$; and (3) from 923 to 1023 K, Ni_2P crystallized. However, when the sample was heated under a flow of pure He, the authors were able to identify the formation of nickel pyrophosphate, α-$Ni_2P_2O_7$, at temperatures close to 673 K.

Berhault et al. [24] investigated the transformation of $NiNH_4PO_4.H_2O \rightarrow Ni_2P$ using *in situ* XRD, *in situ* XAS, and magnetic susceptibility measurements, concluding that the transformation took place in three steps, as earlier suggested by Rodriguez et al. [23] and that the amorphous phase formed in the temperature region 573–673 K was nickel pyrophosphate, α-$Ni_2P_2O_7$. According to the authors, the nickel pyrophosphate phase formed from the decomposition of the nickel ammonium phosphate precursor, simultaneously forming water and ammonia, in agreement with the on-line mass spectroscopy observations of Rodriguez et al. [23]. This decomposition was not accompanied by any changes in the nickel oxidation state, because in both ammonium nickel phosphate and nickel pyrophosphate, the metal has an oxidation state of +2.

Therefore, the main objectives of this work were:

(1) To show that by incorporating small amounts of palladium (0.1%, 0.5% or 1% w/w) into a $Ni_xP_yO_z/SiO_2$ catalyst, it was possible to decrease the synthesis temperature of Ni_2P/SiO_2 from 992 to 772 K. This reduction was likely due to the hydrogen spillover phenomenon that takes place in the palladium particles at low and moderate temperatures.
(2) To show that when a P/Ni ratio of 0.8 is employed, there is the formation of a $Ni_3(PO_4)_2$ phase after the calcination step.

2. Experimental

2.1. Catalyst preparation

2.1.1. Bulk Ni_2P

Bulk Ni_2P, used as reference, was prepared following a two-step procedure as previously described by Wang et al. [25]. In the first step, 35 mL of a $(NH_4)_2HPO_4$ solution (0.054 mol – Nuclear, PA, 99.9%) was added to the same volume of a $Ni(NO_3)_2{\cdot}6H_2O$ solution (0.071 mol – Riedel de Haën, PA, 99.9%) that was maintained under magnetic stirring. After mixing the two solutions, a yellow precipitate was formed that dissolved after the addition of 7 mL nitric acid (Merck). Then, the solution was heated to 363 K, and the temperature was held constant until complete evaporation, resulting in the formation of a yellow-greenish solid. This solid was dried at 433 K for 12 h and then calcined in air at 773 K for 6 h, resulting in a light brown solid, which will be referred to herein as $Ni_xP_yO_z$.

In the second step, $Ni_xP_yO_z$ was reduced to Ni_2P by TPR. In a typical experiment, 0.1 g $Ni_xP_yO_z$ was placed into a U-shaped quartz reactor placed in a furnace (Hoskins) that was controlled by a temperature programmer–controller (Therma – TH2031P model). The temperature was monitored by a chromel–alumel thermocouple positioned near the center of the reactor bed. Prior to the reduction step, the sample was dried under a flow of pure He (50 mL min^{-1}, AGA UP grade, 99.9%) at 773 K for 0.5 h. After the sample was cooled to room temperature (RT), the gas flowing throughout the reactor was switched from pure He to a flow of pure H_2 (100 mL min^{-1}, AGA UP grade, 99.99%), while the temperature was raised from RT to 1173 K at a β of 10 K min^{-1}. During the reduction, the gases coming out of the reactor were passed into a quadrupole mass spectrometer (MKS PPT model) through a leak valve (Granville Phillips), and ions of $m/z = 2$ (H_2), 15 (NH_3), 18 (H_2O), 28 (N_2), 31 (P), 32 (O_2), 34 (PH_3), 44 (CO_2), and 62 (P_2) were

continuously monitored to follow the solid-state transformation $Ni_xP_yO_z \rightarrow Ni_2P$. Because transition metal phosphides are pyrophoric materials, the sample was cooled in a flow of pure He at the end of the synthesis, and when RT was reached, a flow of 0.5% (v/v) O_2/He gas mixture (50 mL min^1 – AGA UP grade) was passed through the reactor for 5 h to passivate the sample and avoid its bulk oxidation during manipulation in the atmosphere.

2.1.2. 30% (w/w) Ni_2P/SiO_2

Similar to unsupported Ni_2P synthesis, the preparation of Ni_2P/SiO_2 followed a two-step procedure: (1) incipient wetness impregnation of the SiO_2 support (Cab-O-Sil M-5, 205 $m^2\ g^{-1}$) followed by calcination, leading to the formation of a compound referred to as $Ni_xP_yO_z/SiO_2$ and (2) the TPR of the $Ni_xP_yO_z/SiO_2$ under a flow of pure H_2 to obtain 30% Ni_2P/SiO_2. The Ni_2P loading of 30 wt.% was chosen based on the work of Sawhill et al. [26].

In the first step, 7.0 g SiO_2 was impregnated using the incipient wetness method by means of a solution resulting from the mixing of $(NH_4)_2HPO_4$ (0.032 mol) and $Ni(NO_3)_2{\cdot}6H_2O$ (0.042 mol). The amounts of $(NH_4)_2HPO_4$ and $Ni(NO_3)_2{\cdot}6H_2O$ were calculated to achieve a theoretical amount of 30% (w/w) Ni_2P after the reduction step. After impregnation, the sample was calcined in air at 773 K for 6 h.

The second step (*i.e.*, the transformation of $Ni_xP_yO_z/SiO_2 \rightarrow$ 30% Ni_2P/SiO_2) was performed by TPR using the procedure described in the previous section. The experiments were done using different heating rates (1, 5 or 10 K min^{-1}). After synthesis, the samples were cooled to RT in a He flow and then passivated for 5 h using a 0.5% (v/v) O_2/He gas mixture (50 mL min^1 – AGA UP grade).

2.1.3. x% (w/w) Pd 30% (w/w) Ni_2P/SiO_2 (x = 0.1, 0.5, 1.0)

The palladium-containing samples were prepared by incipient wetness impregnation of the $Ni_xP_yO_z/SiO_2$ sample with $PdCl_2$ solutions ($PdCl_2{\cdot}2H_2O$, ACROS, 59% Pd) using various amounts of $PdCl_2$ to achieve metal loadings of 0.1%, 0.5%, or 1.0% (w/w) after the reduction step. Briefly, the preparation of 1Pd $Ni_xP_yO_z/SiO_2$ (*i.e.*, the precursor of the 1% Pd 30% Ni_2P/SiO_2 sample) was performed by dissolving 0.084 g $PdCl_2$ in 2.6 mL concentrated HCl, and the resulting solution was evaporated to dryness. Then, 0.74 mL concentrated HCl was added, and after evaporation, 5 mL distilled water was used to dissolve the residue and a second evaporation was performed. Finally, 8 mL distilled water was used to solubilize the residue, and the resulting solution was added dropwise to 4.5 g $Ni_xP_yO_z/SiO_2$ with intermediate drying steps at 373 K for 0.5 h. After all of the palladium solution was impregnated into the $Ni_xP_yO_z/SiO_2$, the sample was dried at 373 K for 1 h and calcined at 773 K for 2 h. Preparation of samples 0.1Pd $Ni_xP_yO_z/SiO_2$ and 0.5Pd $Ni_xP_yO_z/SiO_2$ was performed in a similar manner but employed 0.008 and 0.042 g $PdCl_2$, respectively.

Synthesis of the samples *x*% Pd 30% Ni_2P/SiO_2 (x = 0.1%, 0.5% or 1%) was performed by reducing the respective precursors under a flow of pure hydrogen and employing the same conditions as those described in Section 2.1.2.

2.1.4. Reference catalysts: 30.5% NiO/SiO_2 and 1.15% PdO/SiO_2

Reference samples of 30.5% NiO/SiO_2 and 1.15% PdO/SiO_2 were prepared with Ni and Pd loadings similar to those of the 30% Ni_2P/SiO_2 and 1% Pd 30% Ni_2P/SiO_2 catalysts, respectively. To prepare the 30.5% NiO/SiO_2 sample, 3.8 g SiO_2 was impregnated by incipient wetness with a solution containing 0.042 mol $Ni(NO_3)_2{\cdot}6H_2O$. After the impregnation, the sample was dried at 373 K for 1 h and then calcined at 773 K for 6 h. Preparation of the 1.15% PdO/SiO_2 followed the same procedure as that described in Section 2.1.3, but used pure SiO_2 instead of $Ni_xP_yO_z/SiO_2$ as a support.

2.2. Characterization

2.2.1. N_2 physisorption

Specific surface area (S_g) was determined from nitrogen adsorption isotherms at 77 K using the BET method in an ASAP 2000 (Micromeritics) volumetric apparatus. Before the analyses, the materials were pre-treated under a standard vacuum (6.7×10^{-6} MPa) at 423 K for 20 h.

2.2.2. X-ray fluorescence (XRF)

Analysis of the chemical composition of the samples in their oxidic form was performed using a Rigaku RIX 3100 instrument. Prior to the measurement, the samples were pressed (3000 kgf) in a Carver Laboratory Press (Model C), and the waffles were analyzed for Ni, P, and Pd contents. The results obtained were expressed as weight percentages of NiO, P_2O_5, and PdO. The intensity data of the Pd Kα lines were corrected to the waffle finite thickness using the fundamental parameters method for films. This correction is necessary when an energetic line, such as that of Pd Kα, is present in a matrix of low density.

2.2.3. X-ray diffraction (XRD)

The XRD diffractograms of the samples, either in oxidic or in passivated forms, were obtained in a Rigaku Miniflex diffractometer operated at 45 kV and 40 mA, using Cu Kα monochromatized radiation and a Ni filter. The spectra were recorded in Bragg angles between 20° and 90°, with steps of 0.05° and a counting of 2 s step^{-1}. The crystalline phases in the samples were identified on the basis of the XRD patterns of the JCPDS files.

2.2.4. CO chemisorption

CO-pulsed chemisorption measurements were taken immediately after reduction of the oxidic samples and without exposing them to the atmosphere. These measurements aimed at the titration of the surface metal atoms to estimate the number of active sites of the catalysts. Chemisorption capacity measurements were obtained by pulsing calibrated volumes of CO (AGA, 99.9%) into a He flow and following the m/z = 28 ion in an on-line mass spectrometer (MKS – PPT).

2.2.5. P K-edge in situ X-ray absorption near-edge structure (XANES)

The P K-edge *in situ* XANES measurements were performed at the D04A-SXS beamline in the Laboratório Nacional de Luz Síncrotron (LNLS, Campinas, Brazil), operated in the storage ring mode with a natural emittance of 10 nm rad and a critical energy of 2.08 keV [27]. Synchrotron radiation was monochromatized by a double-crystal monochromator equipped with InSb (1 1 1) crystals, providing an energy resolution of 1 eV at the P K-edge (2145.5 eV). The monochromatic flux was 1×10^{10} photons per energy interval and second. Details of the experimental setup of the beamline have been published elsewhere [27].

The X-ray absorption spectra were recorded in total electron yield (TEY) mode, measuring the electron current at the sample holder with an electrometer connected to the sample. Experiments were performed in a vacuum of 10^{-8} mbar at room temperature. The energy scale was calibrated with a Mo metallic foil, setting the Mo L_3-edge to 2520 eV. All XANES spectra were scanned in the following energy regions: from 2120 to 2135 eV with a width step (w.s.) of 2 eV and an integration time (i.t.) of 2 s, from 2135 to 2165 (w.s. 0.5 eV, i.t. 2 s) and from 2165 to 2200 eV (w.s. 2 eV, i.t. 2 s). The final TEY XANES spectra were obtained after background subtraction and normalization to the post-edge intensity.

Samples were mounted in a vacuum chamber with a background pressure of 10^{-8} mbar, and a pre-chamber was used to perform the different thermal treatments in controlled atmospheres. Fresh samples at the main chamber were analyzed before and after

thermal treatments under 10 mbar of H_2 at 473, 573, 773, and 873 K for 1 h. After each treatment, the samples were transferred in vacuum to the main chamber for the XANES experiment to avoid reaction with oxygen.

The XANES spectra were normalized to perform quantitative analysis of the intensity of the absorption features. The pre- and post-edge regions were fitted by linear and second-order polynomial degree functions, respectively, and then subtracted from the whole spectrum. The absorption jump was set to 1 at a photon energy of ~2170 eV, where the absorption spectra did not exhibit any visible structure.

2.2.6. In situ dispersive X-ray absorption spectroscopy (DXAS)

Ni–K XANES spectra were measured at the D06A–DXAS beamline at LNLS. The curved crystal monochromator selects a bandwidth of hundreds of eV around absorption edges, according to the Bragg angle and radius of curvature. The detection mode was transmission, measured by a charge coupled device (CCD) refrigerated with liquid nitrogen. The detector can operate in two modes: imaging or spectroscopic. In the first mode, it is used to observe a real image in a phosphorous screen (for general optics alignment). In the spectroscopic mode, a full absorption spectra can be acquired in a few milliseconds. Details of the experimental setup of the beamline have been published elsewhere [28]. The spectral data analysis was performed by subtracting a linear background and rescaling the absorbance by normalizing the difference between the baseline and the post-edge absorption in a region approximately 300 eV behind the edge to 1.

Time-resolved spectroscopic studies were performed using a quartz capillary as a flow reactor cell (0.8 mm inner diameter, 0.1 mm wall thickness, 100 mm length), and the schematic experimental setup can be found elsewhere [29]. Samples with particles of ~200 μm in size formed a dense bed throughout which gas flowed with negligible pressure drop and plug-flow hydrodynamics. Heat was supplied by four cartridge heaters mounted inside an insulated copper block. Gases were introduced into the cell from bottles mounted in a portable gas manifold unit with gas purifiers and mass flow controllers. Features of this XAS cell included small sample loading (~10 mg), low flow rates (10 mmol h^{-1}), and plug-flow hydrodynamics, as well as the ability to reach conversions and space velocities similar to those typical of laboratory tubular microreactors. A thermocouple (0.5 mm outer diameter) inserted into the capillary using a metal T-union provided accurate temperature measurements and prevented the sample from being dislodged from the capillary by the flowing gas. During *in situ* measurements, the cell temperatures could be controlled within 1 K (in either temperature-programmed or isothermal modes) using a temperature controller.

2.3. Catalytic testing

Thiophene HDS activity measurements were performed using an atmospheric pressure flow microreactor that was described elsewhere [30]. Activity measurements were performed at a reaction temperature of 593 K over 120 h, using a feed consisting of 3.2 mol% thiophene/hydrogen, which was made by flowing pure H_2 through a saturator filled with thiophene (Merck, 99%) that was kept at 273 K with a refrigerating bath in order to reproduce the conditions employed by Sawhill et al. [26]. The conditions were chosen to have low conversions ($X_T \leqslant 10\%$) and lack diffusion effects (please see Supplementary material for more information).

Prior to catalytic testing, 0.2 g of the sample to be evaluated was reduced under a flow of pure H_2 (200 mL min^{-1}, AGA 99.9%), either at 923 K ($Ni_xP_yO_z/SiO_2$) or at 723 K (*x*% Pd $Ni_xP_yO_z/SiO_2$ and 1Pd/SiO_2), for 1 h. The catalytic evaluation of Ni/SiO_2 followed a different activation procedure, which consisted of sulfiding the oxidic sample with a 5% (v/v) H_2S/H_2 (50 mL min^{-1}; AGA UP) gas mixture at 673 K for 2 h. Once the activation step was completed, the temperature was lowered to 593 K, and the gas flowing through the reactor was switched from pure H_2 (or 5% H_2S/H_2) to the 3.2% mol thiophene/hydrogen gas mixture, initiating the reaction. An automatic valve sampled the gases coming out of the reactor every 15 min and diverted them to a Shimadzu gas chromatograph (GC-17A) equipped with a flame ionization detector and a methylsilicone capillary column (30 m, 250 μm × 1 μm), which allowed complete separation of reactants and products (butane, 1-butene, t-butene, and c-butene). This method allowed calculation of the thiophene conversion and the product selectivity.

Turnover frequency (TOF) values of the samples containing nickel phosphide were calculated using Eq. (1) [31]:

$$\mathrm{TOF} = \frac{F_{Ao}}{W}\frac{X_A}{\mathrm{CO_{uptake}}} \quad (1)$$

where F_{Ao} is the molar rate of thiophene fed into the reactor (μmol s^{-1}), W is the catalyst weight (g), CO_{uptake} is the uptake of chemisorbed CO (μmol g^{-1}), and X_A is the thiophene conversion (%).

3. Results

3.1. Textural properties and chemical composition of the oxidic samples

S_g values for all synthesized samples in their oxidic form are presented in the second column of Table 1. With the exception of the palladium reference sample (1.15% PdO/SiO_2), all of the supported samples had S_g values lower than the SiO_2 employed as the support. Because the SiO_2 was a non-porous material, the observed decrease in S_g might be related to particle agglomeration that likely occurred during the impregnation/calcination steps.

The chemical composition of all supported samples was determined by XRF and is presented in Table 2, with the amounts of Ni, Pd, and P expressed as a weight% of NiO, PdO, and P_2O_5, respectively. The P/Ni molar ratio is also reported in the last column of the table. For samples containing palladium oxide, the determined amount of the noble metal was slightly higher than the theoretical values, and this difference might be due to the model employed to determine PdO content.

XRD diffractograms of SiO_2 and $Ni_xP_yO_z$ presented broad features centered at $2\theta \approx 22°$ and $2\theta \approx 30°$, respectively, indicating that these phases were either amorphous or that the particle size was below the detection limit of the XRD equipment (2 nm) (see Fig. 1 in Supplementary material). However, because this was a bulk material presenting a medium to low surface area, the small particle size hypothesis can be discarded.

Table 1
Specific surface area of the samples in oxidic and passivated states.

Sample	S_g (m^2 g^{-1})	
	Oxidic	Passivated
SiO_2	205	n.m.
$Ni_xP_yO_z/SiO_2$	141	169[a]
0.1Pd $Ni_xP_yO_z/SiO_2$	120	154[b]
0.5Pd $Ni_xP_yO_z/SiO_2$	123	146[b]
1Pd $Ni_xP_yO_z/SiO_2$	93	150[b]
$Ni_xP_yO_z$	53	1[a]
30.5% NiO/SiO_2	155	n.m.
1.15% PdO/SiO_2	217	215[b]

n.m. = not measured.
[a] Reduction up to 923 K at β = 1 K min^{-1}.
[b] Reduction up to 723 K at β = 1 K min^{-1}.

Table 2
Chemical composition (weight%) of the samples in their oxidic state.

Sample	PdO (%)	NiO (%)	P_2O_5 (%)	SiO_2 (%)	P/Ni
$Ni_xP_yO_z/SiO_2$	–	32.28	16.58	51.14	0.54
0.1Pd $Ni_xP_yO_z/SiO_2$	0.15	28.44	17.92	53.49	0.67
0.5Pd $Ni_xP_yO_z/SiO_2$	0.72	28.19	18.56	52.53	0.67
1Pd $Ni_xP_yO_z/SiO_2$	1.63	28.10	17.14	53.13	0.62
30.5% NiO/SiO_2	–	33.63	–	66.37	–
1.15% PdO/SiO_2	1.25	–	–	98.75	–

The diffraction patterns of the $Ni_xP_yO_z/SiO_2$ and *x*% Pd $Ni_xP_yO_z/SiO_2$ samples (see Fig. 1 in Supplementary material) showed a combination of the individual characteristics of both SiO_2 and bulk $Ni_xP_yO_z$. Notably, while the XRD pattern of 1.15% PdO/SiO_2 (Fig. 1 in Supplementary material) presented a small diffraction peak at $2\theta = 33.9°$ because of PdO (PDF 43-1024), the XRD patterns of *x*% Pd $Ni_xP_yO_z/SiO_2$ did not present any diffraction peaks. This observation indicated that palladium has a higher dispersion when impregnated in the $Ni_xP_yO_z/SiO_2$ than when it is impregnated directly into the SiO_2. The reason for poor palladium dispersion on SiO_2 is related to the $PdCl_2$ used as the metal source, a well-known fact in the literature [32].

3.2. Phosphide synthesis by TPR

The water formation profile of the 1.15% PdO/SiO_2 sample obtained during TPR with $\beta = 10\ K\ min^{-1}$ is shown in Fig. 1a and is composed of a single reduction peak with a maximum (T_{max}) at 318 K, indicating that PdO reduction occurred at low temperatures, as expected from previously reported data [32]. The water formation profile for the 30.5% NiO/SiO_2 sample (Fig. 1b) was composed of a shoulder and a peak located at 556 and 603 K, respectively, and was also in accordance with data reported in the literature [33]. While the major reduction peak at 603 K was associated with the reduction of NiO → Ni due to the nickel oxide supported on the SiO_2, the shoulder at 556 K was related to the reduction of bulk NiO particles, which were formed because of the high loading and were not bonded to the support.

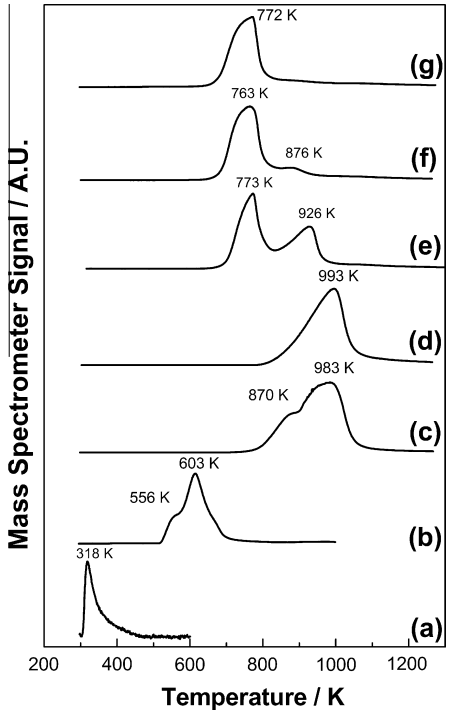

Fig. 1. Water formation profiles during TPR using $\beta = 10\ K\ min^{-1}$ for 1.15% PdO/SiO_2 (a), 30.5% NiO/SiO_2 (b), $Ni_xP_yO_z$ (c), $Ni_xP_yO_z/SiO_2$ (d), 0.1Pd $Ni_xP_yO_z/SiO_2$ (e), 0.5Pd $Ni_xP_yO_z/SiO_2$ (f), and 1Pd $Ni_xP_yO_z/SiO_2$ (g).

Reduction of the $Ni_xP_yO_z$ sample occurred in the temperature range from 800 to 1100 K, and the water formation profile had a shoulder at 870 K and a major peak at 983 K. The observed shoulder and main peak for this sample could indicate that (1) the solid-state transformation of $Ni_xP_yO_z \rightarrow Ni_2P$ proceeded through two steps; (2) the sample was composed of two different phases not detectable by XRD; (3) the sample was composed of particles with different size.

When supported on SiO_2, $Ni_xP_yO_z$ did not present any shoulder in the water formation profile during TPR (Fig. 1d). The TPR profile of the $Ni_xP_yO_z/SiO_2$ sample consisted of an asymmetric peak that presented only one reduction peak with a maximum at $T_{max} = 993$ K. This observation indicated that the solid-state transformation of $Ni_xP_yO_z \rightarrow Ni_2P$ likely occurred in one step. However, when the water formation profiles obtained by TPR for the $Ni_xP_yO_z$ and $Ni_xP_yO_z/SiO_2$ samples were compared, it was found that the temperature ranges of the reductions were nearly identical, thus indicating that the shoulder observed during TPR of the unsupported sample was because of the presence of particles with different size.

Incorporation of different amounts of PdO into the $Ni_xP_yO_z/SiO_2$ sample led to a modification of the shape and the T_{max} value of the water formation profile during TPR. For the lower palladium content (*i.e.*, 0.115% PdO, 0.1% Pd $Ni_xP_yO_z/SiO_2$), the water profile changed from a single peak with a maximum at 993 K (Fig. 1d) to two peaks with maxima at 773 and 926 K (Fig. 1e). Increasing the palladium oxide amount from 0.115% to 0.575% led to a decrease in both the intensity and T_{max} of the second peak from 926 to 876 K, with no modification in the T_{max} value of the first maximum (Fig. 1f). A further increase in palladium oxide content from 0.575% to 1.15% led to the disappearance of the second maximum, resulting in a profile consisting of a single peak with $T_{max} = 772$ K (Fig. 1g). It is important to note that the decrease in T_{max} (~220 K) was independent of the amount of palladium loaded to sample $Ni_xP_yO_z/SiO_2$.

Decreasing the heating rate to 5 or 1 $K\ min^{-1}$ during TPR caused a decrease in the temperature of the maximum of the water formation profiles, as expected from the TPR theory [34]. In the case of $Ni_xP_yO_z/SiO_2$ (Fig. 2a), the decrease of β from 10 to 5 $K\ min^{-1}$ led to a shift in T_{max} from 993 to 949 K; a further decrease in β to 1 $K\ min^{-1}$ was accompanied by a decrease in the maximum to 834 K.

The same effect of the T_{max} shifting to lower temperatures, with decreases in the heating rate, was also observed for *x*% Pd $Ni_xP_yO_z/SiO_2$ samples, as shown in Fig. 2b–d. Aside from the shift of T_{max} to lower values, the decrease in the heating rate during TPR of the 0.1% Pd $Ni_xP_yO_z/SiO_2$ and 0.5% Pd $Ni_xP_yO_z/SiO_2$ samples was accompanied by a decrease in both the intensity and T_{max} of the second reduction peak (Fig. 2b and c, respectively). This effect was not observed for the 1% Pd $Ni_xP_yO_z/SiO_2$ sample because it did not originally present this peak (Fig. 2d). Notably, for a fixed heating rate, the T_{max} value of the first peak in the TPR profiles of the palladium-containing samples depended little on the amount of palladium incorporated into the $Ni_xP_yO_z/SiO_2$.

A close inspection of the water formation profiles presented in Fig. 2 reveals that besides shifting T_{max} to lower temperatures, the decrease in the heating rate also conducts to a diminution of the area under the TPR curves, a fact well explained by the TPR theory [34]. In fact, the signal intensity when integrated over temperature is smaller for lower heating rates, because doing so does not take into account the time spent at each temperature. The diminution of the area under the TPR curves can lead to a false impression that the degree of reduction varies with the heating rate. This is not

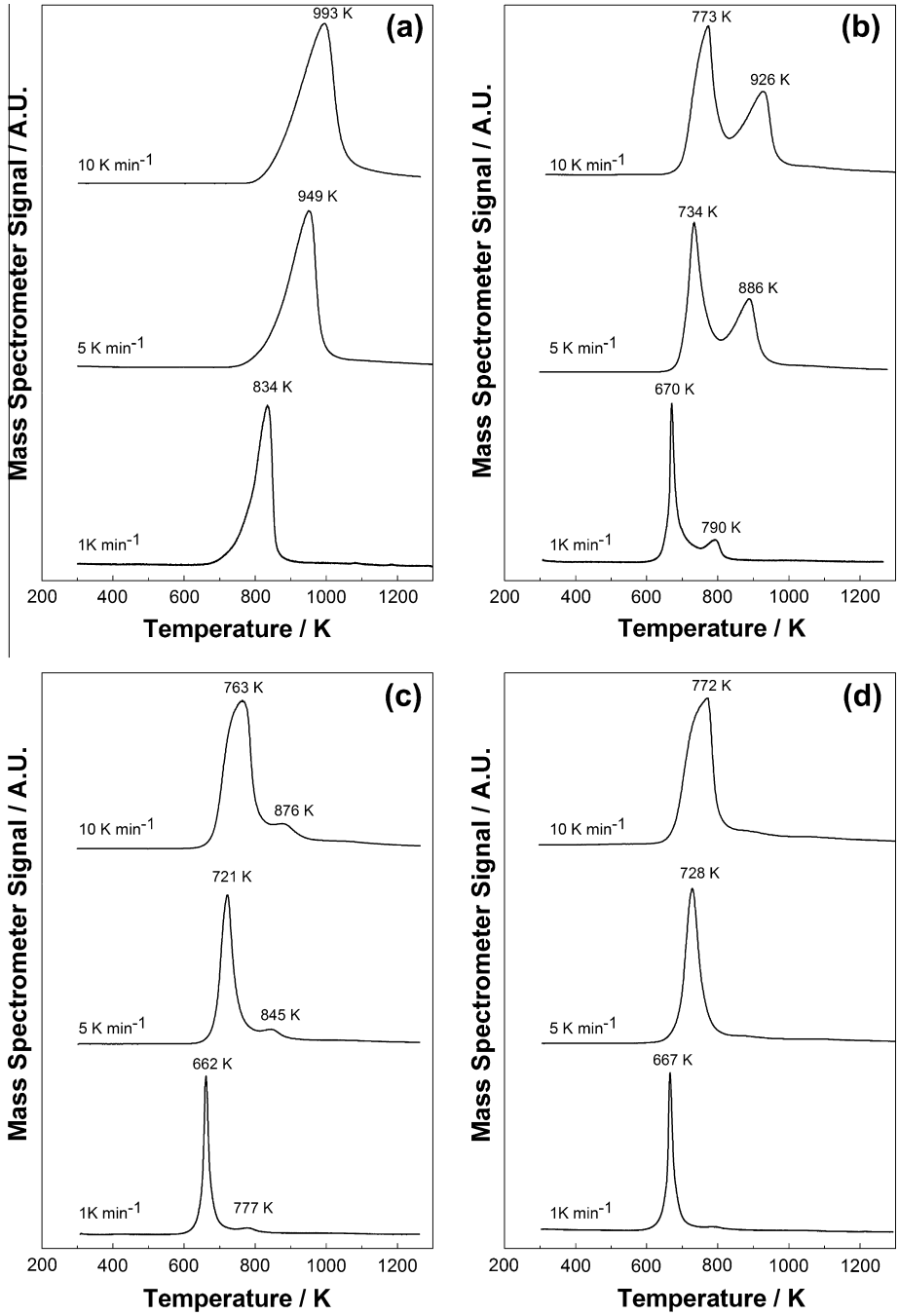

Fig. 2. Water formation profiles using different heating rates during TPR of the samples $Ni_xP_yO_z/SiO_2$ (a), 0.1Pd $Ni_xP_yO_z/SiO_2$ (b), 0.5Pd $Ni_xP_yO_z/SiO_2$ (c), and 1Pd $Ni_xP_yO_z/SiO_2$ (d).

the case because if the signals of Fig. 2 are integrated over time (instead of temperature), then the same areas are found (see Table 1 in Supplementary material), meaning that all of the samples presented the same degree of reduction.

Despite the fact that the decrease in heating rate for the TPR experiments from 10 to 1 K min^{-1} with the $Ni_xP_yO_z/SiO_2$ sample caused a large displacement in the T_{max} value from 993 to 834 K, the lower reduction temperature of 834 K can still be considered high. Therefore, the application of Ni_2P/SiO_2 as a catalyst in reactions of industrial interest is limited. Conversely, incorporation of small amounts of palladium (as low as 0.1% w/w) to the $Ni_xP_yO_z/SiO_2$ favored the decrease in T_{max} from 834 to 670 K, thus allowing industrial *in situ* synthesis and the use of supported nickel phosphide.

3.3. XRD patterns and textural/chemical properties after reduction

The diffraction patterns obtained after reduction and passivation of $Ni_xP_yO_z$, $Ni_xP_yO_z/SiO_2$, and *x*% Pd $Ni_xP_yO_z/SiO_2$ using the conditions chosen from the TPR data and employed before catalytic testing are presented in Fig. 3. The samples without palladium ($Ni_xP_yO_z$ and $Ni_xP_yO_z/SiO_2$) were reduced with H_2 using a β of 1 K min^{-1} and a final temperature of 923 K, whereas those containing palladium (*x*% Pd $Ni_xP_yO_z/SiO_2$) were reduced using the same heating rate of 1 K min^{-1} but with 723 K as the final synthesis temperature.

The diffraction pattern for the product resulting from the reduction of $Ni_xP_yO_z$ is presented in Fig. 3a and shows peaks at 2θ = 40.8°, 44.8°, 47.6°, and 54.4° that are characteristic of bulk Ni_2P (JCPDS

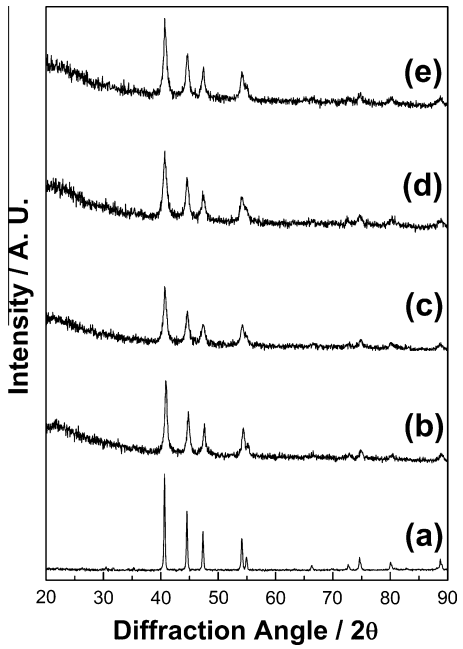

Fig. 3. XRD patterns of Ni_2P (a), Ni_2P/SiO_2 (b),0.1Pd Ni_2P/SiO_2 (c), 0.5Pd Ni_2P/SiO_2 (d), and 1Pd Ni_2P/SiO_2 (e).

74-1385). The supported samples presented a broad feature at $2\theta \approx 22^\circ$ due to the SiO_2 and the characteristic pattern of the bulk Ni_2P (Fig. 3a), indicating that, in all cases, the final product was Ni_2P.

S_g values after reduction and passivation are presented in Table 1. All samples presented lower S_g values than those of the SiO_2 support. Comparing these values to those of the oxidic precursors (third column in Table 1), it can be seen that while the reduction step led to an increase in the S_g value of the supported samples, the S_g value of the bulk sample decreased drastically from 53 to 1 $m^2\ g^{-1}$.

From the TPR profiles it was possible to select the reduction temperatures that should be employed before the catalytic testing for reduction of each of the samples to achieve the formation of Ni_2P. These temperatures were also employed for activation before the CO uptake measurement experiments. The CO chemisorption uptakes are reported in Table 3 and were immediately obtained *in situ*, after the reduction with pure hydrogen at either 923 K ($Ni_xP_yO_z/SiO_2$) or 723 K (*x*% Pd $Ni_xP_yO_z/SiO_2$). The Ni_2P/SiO_2 sample, which was reduced at a higher temperature than the others, presented the highest CO chemisorption uptake value (36 μmol g^{-1}). Notably, samples containing 0.5 and 1 wt.% Pd displayed the same CO uptake (20 μmol g^{-1}), while the sample containing 0.1 wt.% had a CO uptake (15 μmol g^{-1}) equal to that obtained for the 1% Pd/SiO_2 sample.

Table 3
CO chemisorption uptake.

Sample	CO uptake (μmol g^{-1})
Ni_2P/SiO_2	36[a]
0.1Pd Ni_2P/SiO_2	15[b]
0.5Pd Ni_2P/SiO_2	20[b]
1Pd Ni_2P/SiO_2	20[b]
1Pd/SiO_2	15[b]

[a] Reduction up to 923 K at β = 1 K min^{-1}.
[b] Reduction up to 723 K/1 h at β = 1 K min^{-1}.

3.4. In situ XANES and DXAS

K–P XANES spectra for all studied samples are presented in Fig. 4, and for comparison purposes, the spectra of bulk Ni_2P and $Ni_xP_yO_z$ were inserted at the bottom of all other spectra. This figure shows that the K–P XANES spectrum of the Ni_xP_yO/SiO_x sample (Fig. 4a) presented only one absorption peak located at E_o = 2149 eV, which was also observed for the $Ni_xP_yO_z$ sample. This peak was related to the presence of phosphate groups (discussed below). Furthermore, the energy value of 2149 eV was subsequently used as a reference for the energies obtained for all samples at different reduction temperatures (*i.e.*, the incident photon energy is reported as $E - E_o$). The increase in the reduction temperature up to 773 K did not cause any change in the K–P XANES spectrum of $Ni_xP_yO_z/SiO_2$, but for the reduction temperature of 873 K, a second peak at $E - E_o = -8.7$ eV was clearly visible. This peak at −8.7 eV was also observed in the spectrum corresponding to the passivated, unsupported Ni_2P sample (bottom spectrum).

When the K–P XANES spectra of the samples containing palladium (Fig. 4b–d) were analyzed, a small peak at $E - E_o = -8.7$ eV appeared for the reduction temperature of 673 K. The intensity of this peak was augmented with both the temperature and the relative amount of palladium in the sample. Notably, the sample without palladium (Fig. 4a) only presented this peak for temperatures > 773 K. Furthermore, at this temperature of 673 K, the samples containing palladium showed an additional shoulder at $E - E_o = -3$ eV. In contrast, it was clear that the spectrum of the 1% Pd $Ni_xP_yO_z/SiO_2$ sample (Fig. 4d) reduced at 873 K was identical to that of the unsupported Ni_2P, a feature that was shared, to a lesser extent, by the samples containing smaller amounts of the metal (Fig. 4b and c).

The XANES K–Ni edge of the $Ni_xP_yO_z/SiO_2$ and 1Pd $Ni_xP_yO_z/SiO_2$ samples was studied *in situ*, and the results are presented in Fig. 5a and b, respectively. These figures show a decrease in the intensity of the nickel white line and a shift in the absorption line to lower energies with increasing temperature (please note that in these experiments, a heating rate of 10 K min^{-1} was used from RT to 923 K, with a holding time of 1 h due to experimental conditions that did not allow the use of heating rates of 1 K min^{-1}. If it is assumed that a change in the value of the heating rate does not affect the transformation itself but only the maximum temperature where the reduction occurs, then all XANES and DXAS data can still be used, keeping in mind that in these cases the reduction degree is smaller than that obtained in the experiments where lower heating rates were employed). This decrease in white line intensity was associated with a modification of the nickel oxidation state because of the transformation of $Ni_xP_yO_z \rightarrow Ni_2P$. The figures show that although the reduction process of the 1% Pd $Ni_xP_yO_z/SiO_z$ sample began at 670 K and was complete at 720 K (Fig. 5b), the reduction for the sample without palladium was initiated only after spending some time at the final temperature of 923 K (Fig. 5a). Therefore, aside from lowering the reduction temperature, palladium incorporation also led to a decrease in the total time of reduction.

3.5. Thiophene HDS

Catalytic performance in the thiophene HDS reaction at 593 K and atmospheric pressure for the 1% Pd/SiO_2, 30% Ni_2P/SiO_2, and *x*% Pd 30% Ni_2P/SiO_2 samples is presented in Fig. 6. The 30% Ni_2P/SiO_2 catalyst displayed very steady activity during the 120-h reaction, whereas the 1% Pd/SiO_2 catalyst suffered a light deactivation, which was likely either due to the buildup of carbonaceous deposits on its surface or due to the agglomeration of the active phase under the presence of sulfur containing molecules. Conversely, catalysts containing palladium clearly underwent some type of

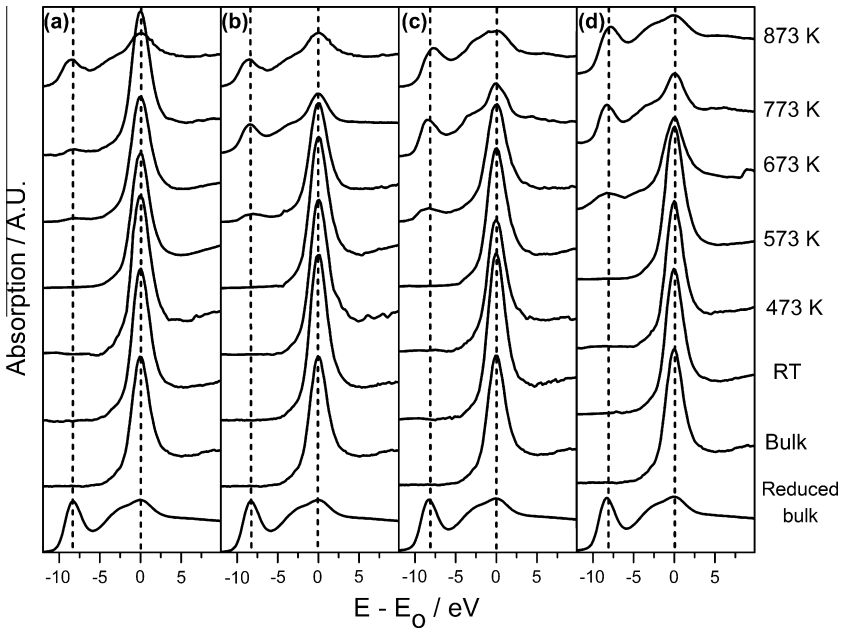

Fig. 4. P–K XANES spectra of samples $Ni_xP_yO_z/SiO_2$ (a), 0.1Pd $Ni_xP_yO_z/SiO_2$ (b), 0.5Pd $Ni_xP_yO_z/SiO_2$ (c), and 1Pd $Ni_xP_yO_z/SiO_2$ (d) at different temperatures under 10 mbar of H_2. Spectra for Ni_2P (reduced bulk) and $Ni_xP_yO_z$ (bulk) reference samples are included for comparison at the bottom.

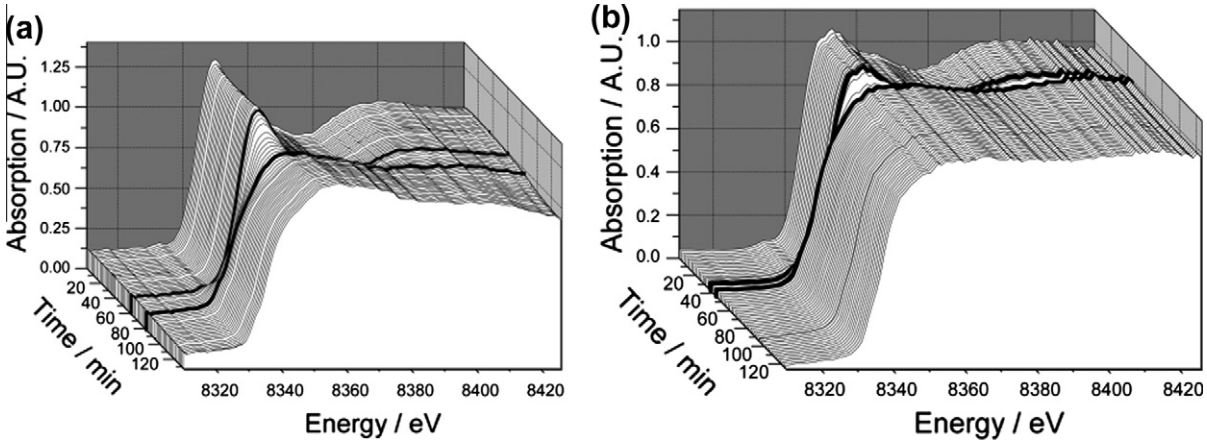

Fig. 5. *In situ* Ni–K XANES spectra of $Ni_xP_yO_z/SiO_2$ (a) and 1Pd $Ni_xP_yO_z/SiO_2$ (b) during temperature-programmed reduction (the highlighted spectra in each set indicate the beginning and the end of the reduction process).

activation during the first 20 h of the reaction, a phenomenon that was more pronounced for the 0.1% Pd 30% Ni_2P/SiO_2 catalyst. Indeed, it is important to note that at the beginning of the reaction, *x*% Pd 30% Ni_2P/SiO_2 catalysts presented a TOF similar to that of 30% Ni_2P/SiO_2, but after a few hours of reaction, all of the noble metal-promoted catalysts presented higher TOF values. For example, after 120 h of reaction, 1% Pd/SiO_2, 0.5% Pd 30% Ni_2P/SiO_2, and 1% Pd 30% Ni_2P/SiO_2 catalysts displayed TOF values roughly twofold greater than that of 30% Ni_2P/SiO_2. Additionally, 0.5% Pd 30% Ni_2P/SiO_2 and 1% Pd 30% Ni_2P/SiO_2 displayed nearly the same TOF. Unexpectedly, the 0.1% Pd 30% Ni_2P/SiO_2 catalyst had a TOF four times larger than that of 30% Ni_2P/SiO_2. Finally, after sulfiding at 673 K, the 30.5% NiO/SiO_2 catalyst (not shown in Fig. 6) suffered a strong deactivation during the course of the reaction, to such a degree that thiophene conversion almost stopped after 100 h of evaluation. However, this phenomenon was not unexpected from previously published reports [26]. The NiO/SiO_2 catalyst was sulfided prior to catalytic evaluation instead of reduced because it is well known in the literature that the active phase in hydrotreating reactions is a sulfide rather than a metal [26].

The selectivity obtained for all of the catalysts is presented in Fig. 7. The most striking feature was that related to butane formation, which demonstrated that despite its light deactivation, the 1% Pd/SiO_2 catalyst displayed the highest selectivity value (~11%) among all of the catalysts (~2%). In particular, if the butane selectivity for this catalyst is compared to those obtained for *x*% Pd 30% Ni_2P/SiO_2 catalysts, then it can be hypothesized that palladium had little effect on the selectivity of the products in the promoted catalysts.

One additional, noteworthy feature is the inversion in selectivity between t-butene and 1-butene obtained for the 1% Pd/SiO_2 and *x*% Pd 30% Ni_2P/SiO_2 catalysts. Although 1% Pd/SiO_2 displayed the selectivity trend t-butene > c-butene > 1-butene > butane, catalysts containing the Ni_2P phase (except 0.1% Pd 30% Ni_2P/SiO_2) presented the trend t-butene > 1-butene > c-butene > butane in the first 80 h of reaction.

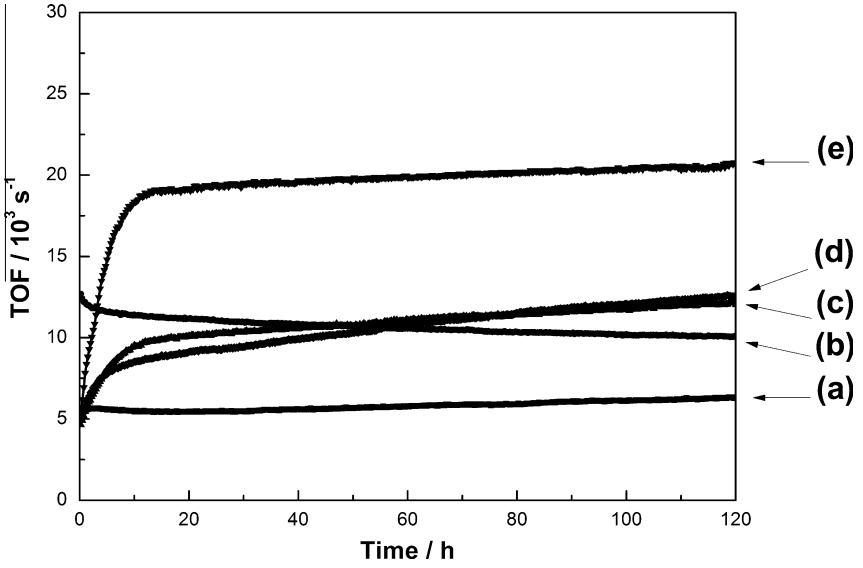

Fig. 6. Catalytic activity of 30% Ni_2P/SiO_2 (a), 1% Pd/SiO_2 (b), 0.5% Pd 30% Ni_2P/SiO_2 (c), 1% Pd 30% Ni_2P/SiO_2 (d), and 0.1% Pd 30% Ni_2P/SiO_2 (e).

Finally, it is also important to note that despite the different tendencies and different initial values, the selectivity for all of the products was nearly the same after 120 h of reaction for all of the catalysts containing the Ni_2P phase.

4. Discussion

If it is assumed that the transformation of $NiNH_4PO_4{\cdot}H_2O \rightarrow \alpha$-$Ni_2P_2O_7$ observed by *in situ* XRD by both Rodriguez et al. [23] and Berhault et al. [24] is purely a thermal phenomenon occurring through the decomposition reaction

$$2NiNH_4PO_4 \cdot H_2O \rightarrow \alpha\text{-}Ni_2P_2O_7 + 3H_2O + 2NH_3 \quad (2)$$

then it is reasonable to assume that the same transformation would occur if a sample was calcined under air at 773 K after the drying step, as was done in the present work. In this way, all of the samples synthesized in this work would be composed of either unsupported nickel pyrophosphate or nickel pyrophosphate supported on silica (*i.e.*, α-$Ni_2P_2O_7/SiO_2$), thus explaining the amorphous character observed by XRD. Moreover, the addition of palladium between 0.1 and 1 wt.% did not lead to any modification of pyrophosphate phase amorphicity.

The hypothesis that an amorphous nickel pyrophosphate phase formed after the calcination step could not be confirmed using the P K-edge XANES spectra of the $Ni_xP_yO_z$ and *x*% Pd $Ni_xP_yO_z/SiO_2$ samples (second and third rows from the bottom in Fig. 4) because both spectra had similar features. These features included an absorption peak located at $E - E_o = 0$ eV ($E_o = 2149$ eV), which could be assigned to the P 1s electronic transition to an unoccupied electronic state formed by the hybridization of the sp^3 and 2p orbitals of P and O, respectively [35]. Thus, the absorption $E - E_o = 0$ eV could be generally assigned to different types of phosphates (PO_4^{-3}, $P_2O_7^{-2}$, P_2O_5), where the P atom was located in the center of a tetrahedron with oxygen atoms at the vertices. This is a limitation of P K-edge XANES because it does not provide enough detail to allow the discrimination of different P forms, as would be observed in the less energetic P $L_{2,3}$-edge XANES as shown by Kruse et al. [36]. A study is currently being conducted in our laboratory using P $L_{2,3}$-edge XANES to discriminate different types of phosphates.

Although reasonable, the hypothesis that α-$Ni_2P_2O_7$ is formed after the calcination step had to be discarded when the chemical compositions reported in Table 2 were closely examined. In fact, if it was assumed that in all samples all of the phosphorous atoms were present as $P_2O_7^{-2}$ species, then the excess of nickel would be in the form of NiO, in compositions varying from 8.6% to 14.8% w/w, as shown in Table 4. Taking into account the surface area of the silica support, these amounts would be high enough to lead to the formation of NiO crystals with sizes that would be detectable by XRD, a fact that was not observed (see Supplementary material).

If a similar reasoning to that employed for nickel pyrophosphate formation but instead considering the formation of $Ni_3(PO_4)_2$ after calcination at 773 K is made, then the theoretical compositions of the samples would be those reported in the third column of Table 4. These values were in much better agreement with the obtained XRD data because the excess nickel would lead to the formation of small amounts of NiO with particle sizes below the XRD detection limit. However, if NiO was present as particles not detectable by XRD, then some evidence would be required to show that $Ni_3(PO_4)_2$ indeed formed an amorphous phase after calcination at 773 K, as previously reported by Robinson et al. [1]. This evidence was indirectly provided by the work of Pérez-Estébanez and Isasi-Marin [37], where the authors synthesized a bulk sample using a similar method to that employed in this work. The samples were calcined in air at different temperatures (823, 923, 973, and 1083 K), and the authors observed that the product calcined at 823 K was amorphous and did not present any XRD peaks, contrary to the others calcined at higher temperatures. Because the lowest calcination temperature employed by Pérez-Estébanez and Isasi-Marin [37] was higher than that used in this work, then it can be assumed that, if formed, the $Ni_3(PO_4)_2$ would be amorphous.

The hypothesis of $Ni_3(PO_4)_2$ formation after calcination at 773 K is further supported by the findings of Sawhill et al. [26]. Indeed, when studying a sample supported on silica with the same amount of Ni_2P and the with the same P/Ni ratio used in this work, these authors concluded from XPS data that the observed binding energy of 133 eV for P ($2P_{3/2}$) was in agreement with the value of 133.3 eV reported by Franke et al. [38] for P in $Ni_3(PO_4)_2$.

The P K-edge spectra presented in Fig. 4 were used to estimate the degree of reduction of the various samples, using the bulk Ni_2P as a reference. The intensities for each of the absorption peaks in Fig. 4 were obtained by means of a least-square fitting routine assuming Gaussian line shape with peaks A_1, A_2, and B_1 (see Fig. 8) and using the WinXAS 3.1 program [39]. The normalization

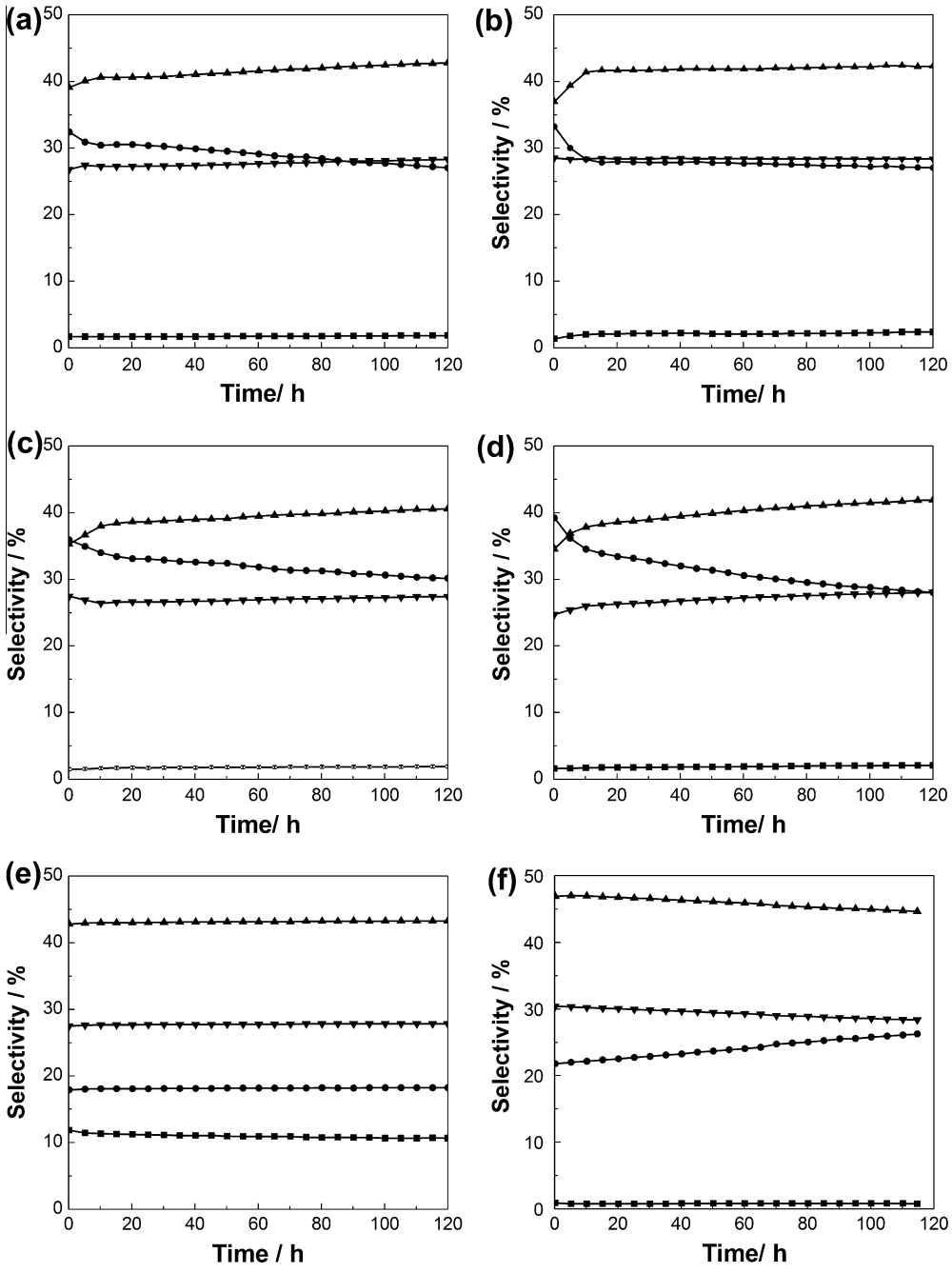

Fig. 7. Butane (■), 1-butene (●), t-butene (▲), and c-butene (▼) selectivity for 30% Ni_2P/SiO_2 (a), 0.1% Pd 30% Ni_2P/SiO_2 (b), 0.5% Pd 30% Ni_2P/SiO_2 (c), 1% Pd 30% Ni_2P/SiO_2 (d), 1% Pd/SiO_2 (e), and 24% Ni/SiO_2 (sulfided at 673 K).

background was fitted assuming an arctan function, with the inflection point at the edge-level energy value (~2149 eV). The ratio R between the first peak (A_1) and the second plus the third peaks ($A_2 + B_1$) (Eq. (3)) is a quantitative estimation of the presence of reduced P species. A reduced bulk sample of Ni_2P was taken as the reference, assuming that the ratio R was equal to 1 for this reference compound.

$$R = \frac{\left(\frac{A_{1,sample}}{A_{2,sample}+B_{1,sample}}\right)}{\left(\frac{A_{2,bulk}}{A_{2,bulk}+B_{1,bulk}}\right)} \quad (3)$$

In Fig. 4, it can be seen that at ambient temperature, all samples had the same P K-edge XANES spectrum, which was similar to that of bulk $Ni_xP_yO_z$. The first modification of the spectra of the palladium-containing samples was in agreement with the XRD and TPR results and occurred at a temperature of 673 K. This phenomenon was reflected in the appearance of a small peak at $E - E_o = -8.7$ eV that was related to the Ni_2P phase and associated with electronic transitions from the 1s level to a mixture of 3p and 3d orbitals from P and Ni, respectively. For treatments at higher temperatures, another peak located at −3 eV appeared, but due to its low intensity, it was not completely defined.

Applying Eq. (3) to the different spectra in Fig. 4 allowed the determination of the degree of reduction, as presented in Fig. 9. This figure shows that the reduction of samples with palladium began at 673 K, and at this temperature, greater amounts of palladium led to a greater degree of reduction. These results were in agreement with those obtained by *in situ* XRD (see Fig. 2 in Supplementary material), where it was shown that Ni_2P formation was

Table 4
Theoretical composition of the samples if all phosphorous atoms were incorporated in either α-$Ni_2P_2O_7$ or $Ni_3(PO_4)_2$ phases.

Sample	If all P atoms were in	
	α-$Ni_2P_2O_7$	$Ni_3(PO_4)_2$
$Ni_xP_yO_z/SiO_2$	34.02% α-$Ni_2P_2O_7$ 14.83% NiO 51.14% SiO_2	42.75% $Ni_3(PO_4)_3$ 6.11% NiO 51.14% SiO_2
0.1Pd $Ni_xP_yO_z/SiO_2$	36.76% α-$Ni_2P_2O_7$ 9.58% NiO 0.15% PdO 53.49% SiO_2	46.21% $Ni_3(PO_4)_3$ 0.15% NiO 0.15% PdO 53.49% SiO_2
0.5Pd $Ni_xP_yO_z/SiO_2$	38.08% α-$Ni_2P_2O_7$ 8.66% NiO 0.72% PdO 52.53% SiO_2	46.75% $Ni_3(PO_4)_2$ 0.00% NiO 0.72% PdO 52.53% SiO_2
1.0Pd $Ni_xP_yO_z/SiO_2$	35.16% α-$Ni_2P_2O_7$ 10.05% NiO 1.63% PdO 53.13% SiO_2	44.20% $Ni_3(PO_4)_2$ 1.04% NiO 1.63% PdO 53.13% SiO_2

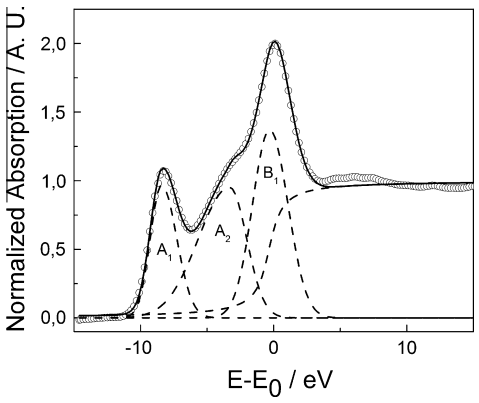

Fig. 8. P–K XANES experimental data (solid circles) and fitted curve (full line). Dotted lines indicate each contribution to the total spectrum. E_o = 2148 eV.

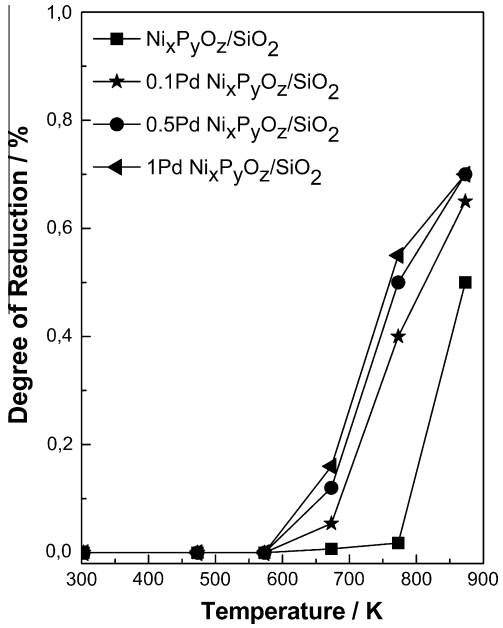

Fig. 9. Degree of reduction of samples $Ni_xP_yO_z/SiO_2$ (a), 0.1Pd $Ni_xP_yO_z/SiO_2$ (b), 0.5Pd $Ni_xP_yO_z/SiO_2$ and (c), 1Pd $Ni_xP_yO_z/SiO_2$ estimated from the P–K XANES data and relative to a bulk Ni_2P sample.

detected only for a reduction temperature of 673 K. According to Fig. 9, at 773 K, >50% of the phosphorous was already reduced in the sample containing 1% palladium, whereas only 2.5% was reduced for the $Ni_xP_yO_z/SiO_2$ sample.

The positive effect of the palladium incorporation in decreasing the reduction temperature was also observed by analyzing the Ni white line. Fig. 10 shows the decrease in the intensity and the shift to smaller energies for the Ni white line during the reduction process. This figure shows that the process initiated at lower temperature and that the necessary time to achieve a certain degree of reduction at a fixed temperature was decreased when palladium was incorporated into the phosphate sample. In fact, Fig. 10 shows that although the reduction of the non-promoted sample ($Ni_xP_yO_z/SiO_2$) only started 12 min after reaching the final reduction temperature of 923 K, the reduction of the 1% Pd $Ni_xP_yO_z/SiO_2$ sample began around 673 K and took only 5 min to achieve the final degree of reduction. These results and temperature values were in agreement with those of TPR (Figs. 1 and 2), where it was clear that for the same heating rate, the palladium-containing samples presented a maximum at temperatures 200 K lower than those without the noble metal, and the reduction process started earlier. This effect of diminishing the reduction temperature could be explained by taking into account the hydrogen spillover phenomenon that occurs in the presence of noble metals [40]: if it is assumed that after impregnation and calcination, the PdO particles were supported in the phosphate phase of the $Ni_xP_yO_z/SiO_z$ sample, then after the reduction of these palladium particles, the hydrogen activation will promote further hydrogen activation and spillover, thus allowing the reduction of the $Ni_3(PO_4)_2$ phase at lower temperatures.

If the P K-edge XANES results are taken into account, then it is clear that the higher the palladium amount, the higher the degree of reduction in the beginning of the process, as shown in Fig. 9. This observation indicates that the extent of the hydrogen spillover was indeed a function of the noble metal concentration. In contrast, at higher reduction temperatures (873 K), Fig. 9 indicates that although samples containing 0.5% and 1% Pd have the same degree of reduction (70%), the sample containing 0.1% Pd has a lower reduction degree (65%).

Another observation that confirms the hypothesis that the hydrogen spillover effect was a function of the palladium loading was found by analyzing the water formation profiles obtained for a fixed heating rate (Fig. 2). For instance, if the profiles obtained for β = 10 K min^{-1} are inspected in Fig. 2, it is clear that, relative to the non-promoted sample ($Ni_xP_yO_z/SiO_2$), the samples containing palladium present a maximum located at temperatures 200 K lower. However, depending on the palladium amount, either two (0.1% and 0.5% w/w Pd samples) or only one reduction peak (1% w/w Pd sample) was present, attributed to more or less hydrogen spillover.

If it is assumed that the palladium particles had roughly the same size after the calcination step, then the higher the noble metal loading, the higher the number of particles available to both promote the hydrogen spillover and increase its extent. Because the 0.1% Pd $Ni_xP_yO_z/SiO_2$ sample had the lowest palladium concentration and therefore the lowest number of available particles, it can be assumed that at the beginning of the reduction process, these particles promoted hydrogen spillover. In this way, the reduction of the $Ni_3(PO_4)_2$ phase began at temperatures 200 K lower than the non-promoted samples. With the progress of the reduction, part or all of the palladium particles were recovered by the Ni_2P-formed phase and because of recovering and/or migration, the hydrogen spillover would stop. Furthermore, without palladium particles available for the spillover, the $Ni_3(PO_4)_2 \rightarrow Ni_2P$ reduction would occur at higher temperatures. If this proposition is true, then the first maximum in the profiles of Fig. 2b was associated with the $Ni_3(PO_4)_2 \rightarrow Ni_2P$ reduction by the activated hydro-

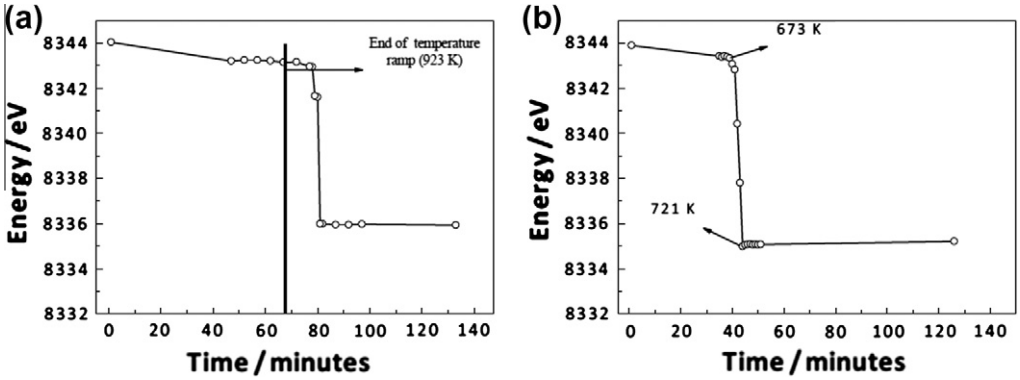

Fig. 10. Edge energy shift for the Ni–K XANES spectra of $Ni_xP_yO_z/SiO_2$ without Pd (a) and with 1 wt.% of Pd (b) sample taken *in situ* conditions during reduction in H_2.

gen, and the second maximum was due to the same transformation occurring only by a temperature effect. According to this hypothesis, the higher the palladium loading, the higher the hydrogen spillover effect and therefore a decreasing amount of $Ni_3(PO_4)_2$ would be thermally reduced. Fig. 11 is a schematic representation of the proposed model for the reduction of promoted and non-promoted samples.

Despite the lack of spectroscopic data to support the assumption of the occurrence of hydrogen spillover on the palladium particles, the hypothesis can be further considered to be true if other works in the literature are took into account. Several reports in the literature show that palladium or platinum incorporation to a MoO_3/Al_2O_3 catalyst lead to a big decrease in the molybdenum oxide reduction temperature [41–43], independently of the palladium source employed (nitrate or chloride), and this effect was attributed to the hydrogen spillover that took place in the noble metal particles. Based on these works, the hypothesis that the hydrogen spillover phenomenon is responsible for the lowering of the $Ni_3(PO_4)_2$ reduction temperature is a reasonable one. However, at the present, the exact mechanism is unknown and further studies have to be performed to completely elucidate it.

Analysis of Fig. 6 reveals that while the 30% Ni_2P/SiO_2 catalyst has a very steady activity over 120 h of reaction, reactions promoted with palladium went through some slow activation process, with activity increasing during the first 20 h of reaction and then reaching steady values. This increase in activity with time on stream has been previously reported for Ni_2P catalysts [23,26,44] and was attributed to a partial sulfidation of the Ni_2P. Using XRD and EXAFS analysis, Oyama et al. [7,45] proposed that during the course of the reaction, a phosphosulfide phase formed on top of the Ni_2P and this phosphosulfide would be the active phase in hydrotreating reactions.

This assumption of phosphosulfide formation during the course of the reaction was also considered in other reports [20,46]. In fact, in a theoretical study using density functional theory calculations, Nelson et al. [47] demonstrated that under hydrotreating conditions, it was possible to replace up to 50% of phosphorous atoms of the (0 0 1) Ni_2P surface with sulfur atoms, forming a Ni_3PS phase that was more energetically stable than bulk Ni_2P or Ni_3S_2. However, although this theoretical study pointed to the maximum amount of sulfur incorporated into the Ni_2P phase, it should be kept in mind that under real reaction conditions, the degree of sulfidation could be lower, as reported by Korányi et al. [44]. In this report, a phosphosulfide was identified with a composition of $Ni_2P_{1.0}S_{0.24}$ after the reaction.

Taking all of these reports into account [7,20,23,26,44,46], it is reasonable to assume that the increase in activity observed for the palladium-promoted samples during the first 20 h of reaction is due to a slow transformation of the Ni_2P into a phosphosulfide phase, $Ni_xP_yS_z$. However, if this assumption is true, two questions immediately arise: (1) Why did the non-promoted sample (*i.e.*, 30% Ni_2P/SiO_2) display steady activity? (2) Why did the promoted samples show different activation behaviors (*i.e.*, samples containing 0.5% and 1% Pd displayed almost the same activities, and the sample with 0.1% Pd showed a higher final activity)?

The answer to both questions relies on the final temperatures used to reduce the oxidic samples. In fact, while the non-promoted sample was reduced prior to the catalytic testing (or CO chemisorptions measurements) under a flow of pure H_2 at 923 K, the promoted samples were reduced using the same experimental conditions but at 723 K as the final temperature. Under these conditions, it is normal to assume that the Ni_2P/SiO_2 and *x*% Pd Ni_2P/SiO_2 catalysts have different degrees of reduction, with the catalysts activated at a higher temperatures resulting in larger degrees of reduction.

When the K–P XANES results were analyzed (Fig. 9), it was found that for a reduction temperature of 723 K, samples containing 0.5% and 1% palladium presented similar degrees of reduction. These degrees of reduction were larger than those of the samples with 0.1% Pd or without palladium. At this point, it is important to note that while the data in Fig. 9 were obtained using a heating rate of 10 K min^{-1}, the heating rate was 1 K min^{-1} during the activation of the samples prior to the catalytic testing. This indicates that the reduction degrees of the samples under reaction conditions were higher than those reported in Fig. 9 with the same trend in the degree of reduction (*i.e.*, 0.5% Pd $Ni_2P/SiO_2 \approx 1\%$ Pd $Ni_2P/SiO_2 > 0.1\%$ Pd Ni_2P/SiO_2). Because the Ni_2P/SiO_2 was obtained using a somewhat more drastic reduction condition (923 K, 1 h), this sample presented a higher degree of reduction.

If it is assumed that CO linearly adsorbs on nickel atoms of the Ni_2P, as theoretically and experimentally shown by Nelson et al. [47] and Layman and Bussel [48], respectively, then the higher the number of nickel atoms available for chemisorption, the higher the CO chemisorption. In other words, higher degrees of reduction would result in higher values of CO chemisorption uptake. When the CO uptake values presented in Table 3 are considered, it can be seen that the proposed trend for the degree of reduction ($Ni_2P/SiO_2 > 1\%$ Pd $Ni_2P/SiO_2 \approx 0.5\%$ Pd $Ni_2P/SiO_2 > 0.1\%$ Pd Ni_2P/SiO_2) is confirmed.

The fact that the different samples presented different degrees of reduction indicates that the residual amount of oxygen in each one of them was different and followed the opposite trend, with the more reduced samples having less residual oxygen in their structures. However, independent of the amount of residual oxygen, all of the samples presented the characteristic X-ray diffraction pattern of the Ni_2P phase after the reduction and passivation steps (Fig. 3). This amount of residual oxygen in the different sam-

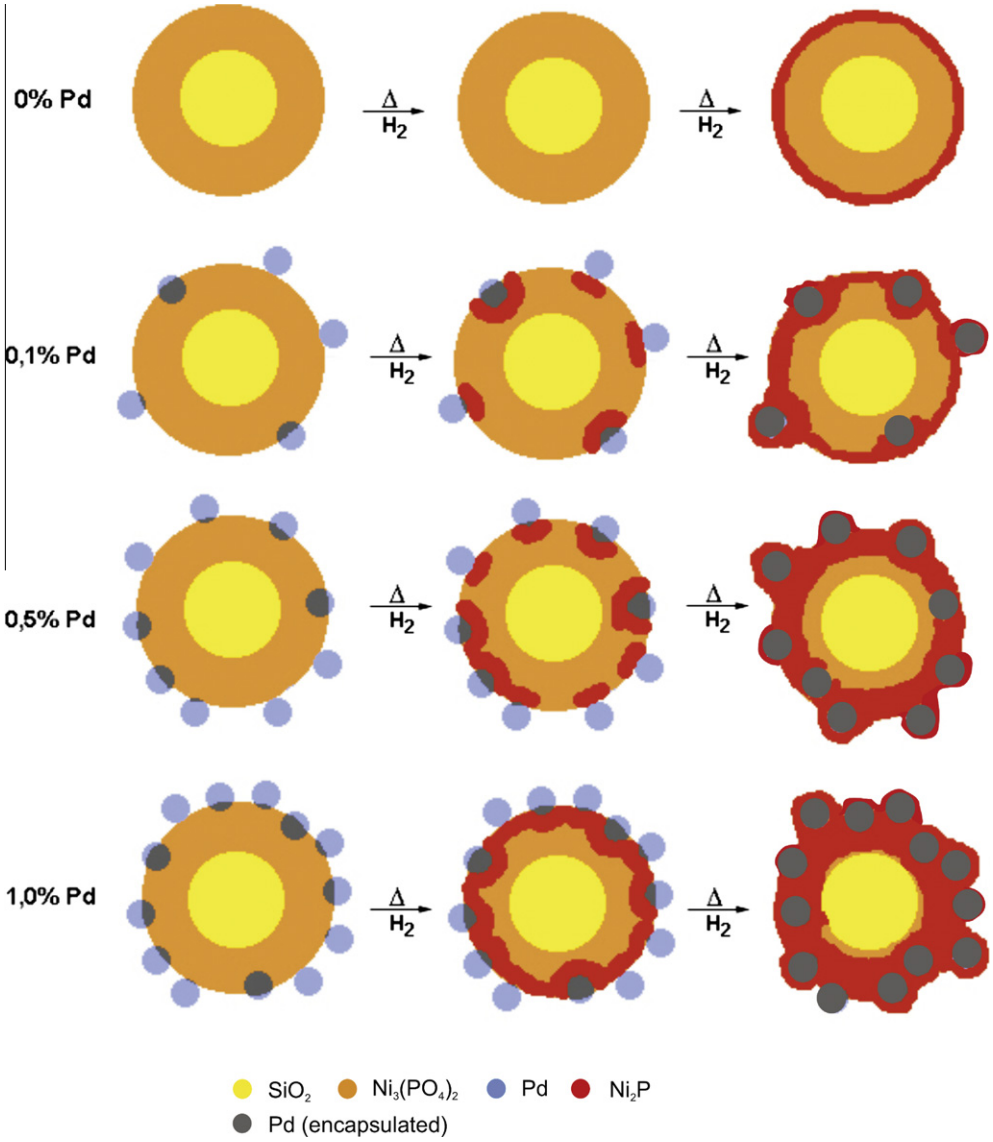

Fig. 11. Proposed model for the reduction of nickel phosphate supported on silica in function of the palladium amount. For a particular reduction temperature, the figure depicts that the higher the palladium content, the higher the occurrence of hydrogen spillover and therefore the higher the phosphate reduction into Ni_2P.

ples seemed to play an important role over the final activity, as discussed next.

Nelson et al. [47] showed that sulfur incorporation into the Ni_2P phase could occur either through the dissociation of the H_2S formed during the reaction or through surface phosphorus replacement by sulfur. In the latter case, the model assumed that there was the removal of a phosphorous atom from the surface in the first step in a very energetic process (E = +1.71 eV), thus creating a vacancy. In the second step, the very reactive vacancy readily reacted with H_2S, leading to the formation of the Ni_3PS and molecular hydrogen. According to their calculations, the replacement of phosphorus by sulfur could only occur for up to 50% of the phosphorous atoms.

The creation of phosphorus vacancies could occur either during the reduction process (if high temperatures were employed) or during the reaction at high hydrogen and H_2S partial pressures. However, none of these situations occurred in the present study. Considering that after the reduction, the samples used in this study had different amounts of residual oxygen ($Ni_2P_yO_{1-y}$), it can then be assumed that the H_2S formed during the thiophene HDS slowly began reacting with oxygen atoms to form a surface phosphosulfide phase ($Ni_2P_yO_{1-y} \rightarrow Ni_2P_yS_{1-y}$). This scenario would explain the observed increase in activity, as the larger the residual oxygen (y close to 0.5 in the partially reduced phosphide, $Ni_2P_yO_{y-1}$), the higher the sulfur incorporation, and consequently, the higher the final catalytic activity. In this way, the observed catalytic activity (0.1% Pd Ni_2P/SiO_2 > 0.5% Pd $Ni_2P/SiO_2 \approx$ 1% Pd Ni_2P/SiO_2 > Ni_2P/SiO_2) could be explained and is in agreement with previous works from the literature that have correlated the catalytic activity of bulk Ni_2P catalysts with the degree of reduction [3,5,11,22,26]. Because the samples with lower degrees of reduction had more residual oxygen that could potentially be replaced by sulfur, then we speculate that fully reducing the phosphate precursor prior to the catalytic testing would not lead to the more active catalyst.

Taking into account that Nelson et al. [45] have proposed in their theoretical work that in pure (0 0 1) Ni_2P half of the phosphorous atoms can be replaced by sulfur in a very energetic process (E = +1.71 eV), what is hypothesized here is that if the phosphide is partially reduced ($Ni_2P_yO_{1-y}$, $y \leqslant 0.5$) prior to catalytic testing, then the replacement of the residual oxygen atoms by sulfur forming a phosphosulfide would be more easy than the direct substitution of a phosphorous atom by sulfur. Moreover, other works in the literature [26,49] have shown that sulfiding the $Ni_xP_yO_z/SiO_2$ at

673 K prior to reduction at 873 K leads to catalysts more active than that only reduced at 873 K.

Another point that could be raised concerning the catalytic behavior of the promoted samples is related to the presence or not of residual chlorine in the surface of the catalysts. In fact, it is well known from the literature that the presence of residual chlorine ions affects the activity of Pd catalysts prepared from $PdCl_2$ supported either on alumina [50] or silica [51]. During the TPR experiments depicted in Figs. 1 and 2, no signal attributed to HCl ($m/z = 36$) was observed by mass spectroscopy, thus indicating either that chlorine is strongly attached to the phosphate phase or that if released, the amount freed from the catalyst was below the detection limit of the mass spectrometer. No matter what hypothesis is true, the surface chemistry of the residual chlorine ions attached to the phosphate phase must be completely different from that on alumina or silica because the XRD data of the oxidic compounds presented in Supplementary material show that while the PdO/SiO_2 sample (see Fig. 1g in Supplementary material) presented a diffraction associated with PdO, the samples *x*% PdO $Ni_xP_yO_z/SiO_2$ did not show any diffractions at all.

If it is assumed that the chlorine ions are attached to the phosphate and remain in the sample even after reduction, then their role over the apparent activity is a matter of further study. However, Guan et al. [19] have shown that the catalytic activity of bulk Ni_2P containing residual amounts of chloride was not affected when compared to a catalysts synthesized by TPR of bulk nickel phosphate. Therefore, it can be inferred from the work of Guan et al. [19] that the presence of residual chloride ions does not affect the activity of nickel phosphide.

At this point, it could be argued that part of the activity presented by the promoted samples was due to the presence of the noble metal. This question cannot be answered solely by analysis of the activity data in Fig. 6, and complementary experiments (*e.g.*, X-ray photoelectron spectroscopy) would have to be performed to determine the surface concentration of palladium. However, when the selectivity data presented in Fig. 7 are considered, then it becomes very clear that palladium had no influence over the catalytic activity because, if it had, the butane selectivity of the promoted samples would be > 10% (please note that the product selectivity was compared at very similar levels of thiophene conversion). Furthermore, the selectivity values of the promoted samples were quite similar to those presented by the non-promoted sample, indicating that the nature of the active sites was similar for all samples.

The comparison of the butane selectivity values of the *x*% Pd Ni_2P/SiO_2 and that of the Pd/SiO_2 reference catalyst was important in proving that palladium was not taking part in the overall reaction. In addition, it validated the model proposed in Fig. 11, where palladium was covered by nickel phosphide during the reduction. In this way, the beneficial effect of the addition of small amounts of palladium to $Ni_xP_yO_z/SiO_2$ catalysts allowed their activation at lower temperatures than those commonly employed.

5. Conclusions

The addition of small amounts of palladium to a supported nickel phosphate on silica ($Ni_xP_yO_z/SiO_2$) led to a decrease of approximately 230 K in the synthesis temperature of Ni_2P. This decrease likely occurred due to hydrogen activation that took place in the palladium particles; this more active form of hydrogen easily reduced the supported nickel phosphate. During the synthesis process, the Pd particles were covered by and/or migrated to the bulk of the Ni_2P and therefore were not available to participate in the thiophene hydrodesulfurization reaction. *In situ* P K-edge XANES was a useful probe to estimate the degree of reduction of phosphates, and there was a correlation between the degree of reduction and the CO chemisorption uptake. Furthermore, there was an increase in the catalytic activity during the reaction that was more pronounced for the less reduced samples, indicating that the formation of the phosphosulfide species was facilitated by the presence of residual oxygen.

Acknowledgments

LAS and RMA acknowledge Conselho Nacional de Desenvolvimento e Pesquisa (CNPq) and Coordenação de Aperfeiçoamento de Pessoal de Nível Superior (CAPES) for the scholarships received which allowed the realization of this work. FGR and LRA acknowledge CONICET (PIP 112-200801-03079) and ANPCYT (PICT-2008-00038). The authors acknowledge LNLS laboratory by partial support (under proposals D04A-SXS-2830 and 3346, and D06A-DXAS-3363). All of the authors are grateful to Dr. Edilson Tamura and Dr. Flavio Garcia for the assistance with the Ni K-edge experiments at the D06A-DXAS beamline. SJAF and LA acknowledge CONICET for the fellowship support.

Appendix A. Supplementary material

Supplementary data associated with this article can be found, in the online version, at doi:10.1016/j.jcat.2011.01.010.

References

[1] W.R.A.M. Robinson, J.N.M. van Gastel, T.I. Korányi, S. Eijsbouts, J.A.R. van Veen, V.H.J. de Beer, J. Catal. 161 (1996) 539.
[2] W. Li, B. Dhandapani, S.T. Oyama, Chem. Lett. (1998) 207.
[3] C. Stinner, R. Prins, Th. Weber, J. Catal. 191 (2000) 438.
[4] S.T. Oyama, P. Clark, V.L.S.T. da Silva, E.J. Lede, F.G. Requejo, J. Phys. Chem. B 105 (2001) 4961.
[5] D.C. Phillips, S.J. Sawhill, R. Shelf, M.E. Bussel, J. Catal. 207 (2002) 266.
[6] P. Clark, X. Wang, S.T. Oyama, J. Catal. 207 (2002) 256.
[7] S.T. Oyama, J. Catal. 216 (2003) 343.
[8] P. Clark, W. Li, S.T. Oyama, J. Catal. 200 (2001) 140.
[9] S.T. Oyama, P. Clark, X. Wang, T. Shido, Y. Ywasawa, S. Hayashi, J.M. Ramallo-López, F.G. Requejo, J. Phys. Chem. B 106 (2002) 1913.
[10] P. Clark, X. Wang, P. Deck, S.T. Oyama, J. Catal. 210 (2002) 116.
[11] X.Q. Wang, P. Clark, S.T. Oyama, J. Catal. 208 (2002) 321.
[12] A.W. Burns, K.A. Layman, D.H. Bale, M.E. Bussel, Appl. Catal. A 343 (2008) 68.
[13] A.R. West, Solid State Chemistry and its Applications, Wiley, Chichester, 1992. p. 203.
[14] M. Chene, Ann. Chim. 15 (1941) 187.
[15] X.F. Qian, X.M. Liu, Y.T. Qian, J. Solid State Chem. 149 (2000) 88.
[16] J. Park, B. Koo, K.Y. Yoon, Y.H. Wang, M. Kang, J.G. Park, T. Hyeon, J. Am Chem. Soc. 127 (2005) 8433.
[17] C.M. Lukehart, S.B. Milne, S.R. Stock, Chem. Mater. 10 (1998) 903.
[18] C. Stinner, Z. Tang, M. Haouas, Th. Weber, R. Prins, J. Catal. 208 (2002) 456.
[19] Q. Guan, W. Li, M. Zhang, K. Tao, J. Catal. 263 (2009) 1.
[20] J.A. Cecilia, A. Infates-Molina, E. Rodriguez-Castellon, A. Jimenez-Lopez, J. Catal. 263 (2009) 4.
[21] H. Loboué, C. Guillot-Deudon, A.F. Popa, A. Lafond, B. Rebours, C. Pichon, T. Cseri, G. Berhault, C. Geantet, Catal. Today 130 (2008) 63.
[22] S. Yang, R. Prins, Chem. Commun. 33 (2005) 4178.
[23] J.A. Rodriguez, J.-Y. Kim, J.C. Hanson, S.J. Sawhill, M.E. Bussel, J. Phys. Chem. B 107 (2003) 6276.
[24] G. Berhault, P. Afanasiev, H. Loboue, C. Geantet, T. Cseri, C. Pichon, C. Guillot-Deudon, A. Lafond, Inorg. Chem. 48 (2009) 2985.
[25] X. Wang, P. Clark, S.T. Oyama, J. Catal. 208 (2002) 321.
[26] S.J. Sawhill, D.C. Phillips, M.E. Bussel, J. Catal. 215 (2003) 208.
[27] A.R.D. Rodrigues, A.F. Craievich, C.E.T. Gonçalves da Silva, J. Synchrotron Rad. 5 (1998) 1157.
[28] H.C.N. Tolentino, J.C. Cezar, N. Watanabe, S. Piamonteze, N.N. Souza Neto, E. Tamura, A.Y. Ramos, R.T. Neuenchwander, Phys. Scr. T115 (2005) 977.
[29] S.J.A. Figueroa, Ph.D. Thesis, Universidad Nacional de La Plata, La Plata, 2009.
[30] V.L.S.T. da Silva, R. Frety, M. Schmal, Ind. Eng. Chem. Res. 33 (1994) 1692.
[31] J.S. Lee, S. Locatelli, S.T. Oyama, M. Boudart, J. Catal. 125 (1990) 157.
[32] F. Bozon-Verduraz, E.A. Aales, G. Bugli, A. Ensuaque, M.D. Mendes, Phys. Chem. Chem. Phys. 3 (1999) 491.
[33] C. Louis, Z. Cheng, M. Che, J. Phys. Chem. 97 (1993) 5703.
[34] J.L. Falconer, K.A. Schwartz, Catal. Rev. Sci. Eng. 25 (1983) 141.
[35] R. Franke, Spectrochim. Acta A 53 (1997) 933.
[36] J. Kruse, P. Leinweber, K.-U. Eckhardt, F. Godlinski, Y. Hu, L. Zuin, J. Synchrotron Rad. 16 (2009) 247.

[37] M. Pérez-Estébanez, J. Isasi-Marín, J. Sol-Gel Sci. Technol. 47 (2008) 326.
[38] R. Franke, T. Chasse, P. Streubel, A. Meisel, J. Electr. Spectrosc. Relat. Phenom. 56 (1991) 381.
[39] T. Ressler, J. Synchrotron Rad. 5 (1998) 118.
[40] M. Boudart, Chem. Rev. 95 (1995) 661.
[41] M. Schmal, M.A.S. Baldanza, M.A. Vannice, J. Catal. 185 (1999) 138.
[42] M.A.P. da Silva, R.A.M. Vieira, M. Schmal, Appl. Catal. A. 190 (2000) 177.
[43] F.B. Noronha, M.A.S. Baldanza, R.S. Monteiro, D.A.G. Aranda, A. Ordine, M. Schmal, Appl. Catal. A. 210 (2001) 275.
[44] T.I. Korányi, Z. Vít, D.G. Poduval, R. Ryoo, H.S. Kim, E.J.M. Hensen, J. Catal. 253 (2008) 119.
[45] S.T. Oyama, X. Wang, Y.-K. Lee, K. Bando, F.G. Requejo, J. Catal. 210 (2002) 207.
[46] T. Kawai, K.K. Bando, Y.-K. Lee, S.T. Oyama, W.–J. Chun, K. Asakura, J. Catal. 241 (2006) 20.
[47] A.E. Nelson, M. Sun, A.S.M. Junaid, J. Catal. 241 (2006) 180.
[48] K.A. Layman, M.E. Bussell, J. Phys. Chem. B 108 (2004) 15791.
[49] Y. Teng, A. Wang, X. Li, J. Xie, Y. Wang, Y. Hu, J. Catal. 266 (2009) 369.
[50] F. Bozon-Verduraz, A. Omar, J. Escard, B. Pontvianne, J. Catal. 53 (1978) 126.
[51] J. Sepúlveda, N. Fígoli, React. Kinet. Catal. Lett. 53 (1994) 155.